

Study of Crystallization and Composition on Silicon Oxycarbide (SiOC) and Silicon Boron Oxycarbide (SiBOC) Ceramics Obtained from Alkoxysilanes Precursors

Mariana G. Segatelli,^{1b} ^a Patricia M. Sanchez,^a Livia R. C. Silva,^a Maria A. Silva,^a
César R. T. Tarley,^{1b} ^{*a} Paulo R. C. da Silva^b and Emerson S. Ribeiro^{1b} ^c

^aDepartamento de Química, Universidade Estadual de Londrina (UEL),
Rodovia Celso Garcia Cid, PR 445, km 380, 86057-970 Londrina-PR, Brazil

^bDepartamento de Física, Universidade Estadual de Londrina (UEL),
Rodovia Celso Garcia Cid, PR 445, km 380, 86057-970 Londrina-PR, Brazil

^cInstituto de Química, Universidade Federal do Rio de Janeiro (UFRJ),
Avenida Athos da Silveira Ramos, 149, 21941-909 Rio de Janeiro-RJ, Brazil

This work deals on the preparation of silicon oxycarbide (SiOC) and silicon boron oxycarbide (SiBOC) ceramics from pyrolysis involving alkoxysilanes with different organic groups. Boron content, organic substituent and annealing time were evaluated on crystallization and composition of resulting ceramics. B-free precursors composed of methyltriethoxysilane (MTES), phenyltriethoxysilane (PTES) and vinyltrimethoxysilane (VTMS) were obtained by the sol-gel method, whilst B-containing precursors were prepared by adding to each alkoxysilane a proper amount of boric acid resulting in B/Si atomic ratios of 0.1 and 0.5. Precursors were pyrolyzed at 1500 °C for 1 and 3 h to produce respective SiOC and SiBOC ceramics. X-ray diffraction (XRD) patterns revealed enhanced SiC phase crystallization for PTES-derived ceramics, followed by those containing vinyl and methyl groups, which was also confirmed by X-ray photoelectron spectroscopy (XPS) from percentages of Si–C and Si–O bonds. Csp² and Csp³ amounts varied among ceramics, indicating direct influence of organic substituent on conductive carbon phase development. Boron addition induced the growth of SiC crystallites, having more evident effect in matrices with higher proportions of amorphous fraction and lower residual carbon amounts. Organic group nature, boron content and annealing time played an important role for production and evolution of SiC and C phases into ceramics.

Keywords: polymer-derived ceramics, boron, sol-gel method, annealing, free carbon phase

Introduction

Silicon oxycarbide (SiOC) based materials have attracted great attention in Si-polymer derived ceramics (PDCs) field due to their excellent mechanical, thermal, electrical, optical, oxidation resistance and low densities properties.^{1,2} These characteristics make them suitable in a wide application range including high resistance SiOC fibers and ceramic matrix composites,^{3,4} high-temperature receivers and ceramics for thermal insulation,^{5,6} Li-ion batteries and voltammetric sensors,^{7,8} platforms for integrated photonics and luminescent thin films,^{9,10} ceramic coatings for anti-oxidation performance as well as protective layers for high-temperature corrosion,^{11,12}

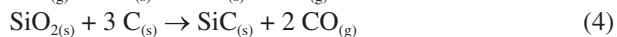
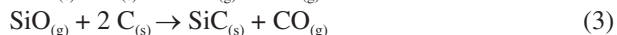
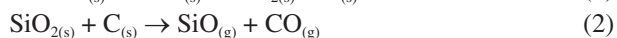
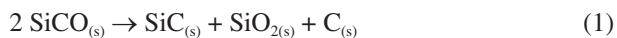
ceramic membranes for water purification and ceramic foams,^{13,14} among others.

SiOC materials are usually prepared by controlled pyrolysis of poly(organosiloxanes) precursors, under inert atmosphere.¹⁵⁻¹⁸ Their micro/nanostructures widely change according to molecular architecture and composition of selected precursors together with pyrolysis conditions such as temperature, isothermal annealing, atmosphere, and heating/cooling rates.^{17,19}

In general, when poly(organosiloxanes) are thermally heated from 800 to 1000 °C, a mixed amorphous ceramic network composed mainly by random arrangements of Si sites tetracoordinate with O and C atoms, commonly described as SiO_xC_{4-x}, 0 ≤ x ≤ 4, is obtained. Furthermore, polyaromatic carbon species are continuously produced into ceramic matrix due to incomplete thermal degradation

*e-mail: tarley@uel.br

of organic groups attached to polymeric chain. This gives rise a second phase in SiOC matrices, named as free carbon (C_{free}), which is constituted by a carbon atoms network in sp^3 and sp^2 hybridizations.^{20,21} At temperatures higher to 1000 °C, homogeneous amorphous matrix undergoes structural transformations promoted by the redistribution reactions among the different Si sites, until a phase separation process is achieved. Around 1300 °C, SiOC begins to decompose, resulting in SiC, SiO₂ and C phases (equation 1).²² As the temperature arises, carbothermal reduction reaction is favored, basically yielding SiC from reaction between free carbon and SiO₂ or Si–O-rich sites, as represented by partials (equations 2 and 3) and global (equation 4) equations.¹⁵ Indeed, at high temperatures, two interpenetrating nanosized networks composed of SiO₂-rich and C-rich regions, in which the latter comprises SiC nanocrystals and graphitic carbon structures, are usually obtained, whose proportions are dependent on the precursor chemistry.²³ According to Kleebe *et al.*,²⁴ at high temperatures such as 1450 °C, the phase separation process involves SiO₄ and SiC₄ rich regions encapsulated by carbon, which initially are composed of finely dispersed graphene layers, and after grow form thicker multi-layer carbon. Such structural arrangement, mainly regarding the existence of free carbon network, justified the thermal stability on mechanical property of SiOC materials.



The incorporation of heteroatoms such as boron into poly(organosiloxanes) can be successfully performed because their molecular structures can be easily tailored. This approach consists in a strategy for producing multicomponent ceramics, besides promotes structural and compositional changes, resulting in characteristics and improved properties of final materials. Specifically, in the SiOC system, B addition leads to the production of silicon boron oxycarbide (SiBOC), which reveals improved high temperature stability, creep resistance and thermooxidative stability when compared to SiOC.^{25,26}

SiBOC materials can be produced cheaply from easily accessible starting reagents. These include alkoxysilanes that assume the general formula $R'_x\text{SiZ}_{4-x}$ ($x = 1, 2, 3$, where R' is an organic group and $Z =$ methoxy, ethoxy groups, among others) and boric acid, B(OH)_3 , SiO₂/B₂O₃ powders, borane dimethylsulfide and triethylborate have already been employed as boron sources,²⁷⁻²⁹ meanwhile B(OH)_3 is the

cheapest source, easily available, nontoxic resource and usually chosen to produce boron-containing ceramics.³⁰⁻³²

Alkoxysilanes and boric acid readily react through hydrolysis and polycondensation reactions involving the sol-gel chemistry, in the absence of solvent. As a result, B is homogeneously incorporated into siloxane network as trigonal BO₃ units via Si–O–B borosiloxane bonds, leading to the formation of amorphous SiBOC ceramics with a mixed network composed of silicon oxycarbide ($\text{SiO}_x\text{C}_{4-x}$, $0 \leq x \leq 3$) and boron oxycarbide ($\text{BO}_y\text{C}_{3-y}$, $0 \leq y \leq 2$) units at around 1000 °C. The excellent high-temperature properties described for SiBOC are attributed to their highly crosslinking structures according to formed Si–O–B bonds.^{20,30,33}

It is reported that boron incorporation into SiOC matrices contributes to the consumption of silicon oxycarbide units, favoring the ceramic matrix crystallization by means of semiconducting β -SiC phase development, besides inhibits the amorphous SiO₂ phase formation.^{32,34} Besides enhanced SiC production, B incorporation revealed significant effect on free carbon graphitization, resulting in SiBOC ceramics with highly graphitized C_{free} and high ceramic yields.^{30,35}

As mentioned before, precursor chemistry has influence over resulting ceramics structure and composition. Specifically, both amounts and distributions of C_{free} phase produced into ceramic matrix during pyrolysis depend on the organic group bonded to Si-polymer precursor. Organic substituents containing unsaturation, such as phenyl and vinyl groups usually give rise to PDCs with higher C_{free} amounts when compared to saturate groups (e.g., methyl and ethyl).^{36,37} As carbothermal reduction reaction (equation 4) reveals a certain dependence with the C_{free} availability, it is expected that higher carbonaceous phase contents contribute to more effective SiC crystallization into ceramic matrices. Therefore, the combined use of boron in alkoxysilanes-based precursors containing different organic substituents shows an important role to manufacture multicomponent PDCs, mainly focusing on the improvement of their electric features due to crystalline phases potentially produced *in situ*. Although some works have already reported the boron addition into alkoxysilanes to produce hybrid $\text{RSiO}_{1.5}/\text{B}_2\text{O}_3$ gels ($R =$ methyl (Me), ethyl (Et), vinyl (Vi)),^{28,38} SiBOC glasses and ceramic fibers,^{35,39,40} ceramic matrix composites (CMCs) involving SiBOC and carbon fibers (C/SiBOC)⁴¹ as well as to evaluate the structural evolution^{30,34,42} and mechanical properties²⁵ of ceramics employing different temperatures, few efforts have been made concerning a comparative study about its simultaneous use into different modified silicon alkoxides and isothermal annealing over ceramics crystallization at high temperatures.

This work reports the synthesis of SiBOC ceramics at 1500 °C from three polymer precursors, prepared by the sol-gel method, involving methyltriethoxysilane (MTES), phenyltriethoxysilane (PTES) and vinyltrimethoxysilane (VTMS) with different B/Si atomic ratios. Corresponding B-free ceramics (SiOC) were also obtained for comparison. The influence of boron content, organic substituent and isothermal annealing on phase crystallization and composition of resulting ceramics was described.

Experimental

Starting reagents

Methyltriethoxysilane (MTES), phenyltriethoxysilane (PTES), vinyltrimethoxysilane (VTMS) (Sigma-Aldrich Ltda, São Paulo, Brazil) and boric acid (H_3BO_3) as boron source (Vetec, Duque de Caxias, Brazil) were used to prepare all preceramic precursors. Hydrochloric acid (HCl) (Vetec, Duque de Caxias, Brazil) and ammonium hydroxide (NH_4OH) (Sigma-Aldrich Ltda, São Paulo, Brazil) were employed during hydrolysis and condensation reactions. All the reagents were used as received without any further purification.

Synthesis of SiOC and SiBOC preceramic precursors

B-free and B-containing samples were prepared by the sol-gel method using MTES, PTES, VTMS and boric acid, according to procedure previously described in literature.³⁴

SiBOC precursors were synthesized by adding to each modified alkoxysilane, MTES, PTES and VTMS, a proper amount of boric acid (H_3BO_3), followed by stirring until their complete dissolution. Compositions containing B/Si atomic ratios of 0.1 and 0.5 were prepared. After dissolution, the obtained clean solutions were cast into Teflon molds, followed by gelation step. The wet B-containing precursors were dried for at least 10 days at 70 °C. For comparison, B-free samples, corresponding to SiOC precursors, were prepared by hydrolysis and condensation reactions, in which each alkoxysilane was hydrolyzed using a H_2O :silane molar ratio of 1:1, at 70 °C for 15 min, under 1.0 mol L⁻¹ HCl solution. Afterward, the acid solutions were neutralized by addition of a stoichiometric amount of NH_4OH solution (30%). The sols were then gelled and dried for at least 10 days at 70 °C.³⁴

After obtainment, all B-free and B-containing precursors were grinded and sieved in $\leq 106 \mu m$ sizes (Bertel Industry Metallurgica Ltda, Caieiras, Brazil) to get better control of the particles sizes before characterization. Table 1 illustrates the codes assigned to all preceramic polymers prepared.

Table 1. Codes corresponding to preceramic polymers prepared by the sol-gel method using MTES, PTES, VTMS and boric acid, in B/Si atomic ratios of 0, 0.1 and 0.5

Alkoxysilane	B/Si atomic ratio	Preceramic polymer
MTES	0	MTES ₀
	0.1	MTES _{0.1}
	0.5	MTES _{0.5}
PTES	0	PTES ₀
	0.1	PTES _{0.1}
	0.5	PTES _{0.5}
VTMS	0	VTMS ₀
	0.1	VTMS _{0.1}
	0.5	VTMS _{0.5}

MTES: methyltriethoxysilane; PTES: phenyltriethoxysilane; VTMS: vinyltrimethoxysilane.

Obtainment of SiOC and SiBOC ceramics

SiOC and SiBOC ceramic materials were obtained by controlled pyrolysis of each polymer precursor employing a high temperature furnace containing an adapted alumina tube (EDG10P-S, São Carlos, Brazil). Pyrolysis procedure was carried out under argon atmosphere, from room temperature up to 1500 °C, with a heating/cooling rate of 5 °C min⁻¹ and annealed for 1 and 3 h at final temperature. Therefore, eighteen ceramic materials based on SiOC and SiBOC systems containing different B/Si atomic ratios, types of alkoxysilanes and annealing times were obtained, as illustrated in Table 2. The choice of pyrolysis temperature at 1500 °C is related to development of crystalline phases, mainly composed of graphitic carbon structures and nanosized SiC crystallites, via carbothermal reduction reaction.^{43,44} Annealing conditions usually contribute to more effective crystallization into ceramic matrices.^{42,45} Therefore, the association between pyrolysis at 1500 °C

Table 2. Codes illustrating general representations for SiOC and SiBOC ceramics obtained from the same alkoxysilane and for each set of ceramics with different B/Si atomic ratios and annealing times

Preceramic polymer	General codes for SiOC and SiBOC ceramics	Code for ceramics after annealing	
		1 h	3 h
MTES ₀	CMS	CMS _{0_1h}	CMS _{0_3h}
MTES _{0.1}		CMS _{0.1_1h}	CMS _{0.1_3h}
MTES _{0.5}		CMS _{0.5_1h}	CMS _{0.5_3h}
PTES ₀	CPS	CPS _{0_1h}	CPS _{0_3h}
PTES _{0.1}		CPS _{0.1_1h}	CPS _{0.1_3h}
PTES _{0.5}		CPS _{0.5_1h}	CPS _{0.5_3h}
VTMS ₀	CVS	CVS _{0_1h}	CVS _{0_3h}
VTMS _{0.1}		CVS _{0.1_1h}	CVS _{0.1_3h}
VTMS _{0.5}		CVS _{0.5_1h}	CVS _{0.5_3h}

and different annealing times plays an important role to investigate the production and growth of C and SiC phases under boron influence.

Characterization techniques

Thermogravimetry (TG)

Thermal stability of preceramic precursors was evaluated on a thermogravimetric analyzer (TGA, 4000, PerkinElmer, Tokyo, Japan) employing a temperature range from 25 to 900 °C, at 10 °C min⁻¹ and nitrogen flowing of 20 mL min⁻¹. Thermogravimetric measurements were conducted with ca. 10 mg of samples and the ceramic yield was obtained by residual mass percentage at final temperature of 800 °C.

Fourier transform-infrared spectroscopy (FTIR)

FTIR spectra of the preceramic polymers and ceramics based on SiOC and SiBOC systems were acquired on a Fourier transform infrared spectrometer (IR Prestige-21, Shimadzu, Tokyo, Japan), between 4000 and 400 cm⁻¹, with spectral resolution of 4 cm⁻¹ and 16 scans. Powdered samples were mixed with KBr pellets and analyzed in the transmittance operation mode.

X-ray diffraction (XRD)

X-ray diffractograms of the SiOC and SiBOC ceramics were obtained on an X-ray diffractometer (PANalytical, X'Pert PRO MPD, Malvern Panalytical, Almelo, Netherlands) operating with Cu K α radiation ($\lambda = 1.54060 \text{ \AA}$), using the θ -2 θ technique, Bragg Brentano geometry at 40 kV and 30 mA. XRD patterns were collected between 5 and 80° (2 θ), with 0.04° step size at 2.0 s. To avoid preferred orientations in the sample preparation process, the powdered samples were rotated cyclically during measurements with a period of 1.0 s.

The average crystallite size (t) for SiC phase was calculated by the Scherrer formula according to equation 5.⁴⁶

$$t = \frac{K \cdot \lambda}{\beta \cdot \cos\theta} \quad (5)$$

where t is assigned to the average crystallite size, λ is the radiation wavelength in nanometers (0.15406 nm), β is the width at half height of the diffraction signal in radians, θ corresponds to half of the 2 θ angle and K is a constant that depends on the particle morphology and ranges from 0.89 to 1.39 rad. As the crystallites obtained in this study have no defined shape, we employed $K = 1$, which corresponds to an apparent average volume size regardless of specific morphology.²⁹⁻³¹

X-ray photoelectron spectroscopy (XPS)

X-ray photoelectron spectroscopy (XPS) measurements were carried out for the SiOC and SiBOC ceramics on a spectrometer (Escalab 250Xi, Surface Analysis Thermo Fischer Scientific, East Grinstead, UK) employing Al K α radiation of 1486.6 eV and survey power of 100 eV. The overall instrumental resolution was about 25 eV. The data were collected by means of an Avantage Data Acquisition and Processing software.

Results and Discussion

SiOC and SiBOC preceramic precursors: macroscopic appearances and characteristics

Preceramic polymers containing methyl-, phenyl- and vinyl-modified alkoxy silanes were synthesized by the sol-gel method, resulting in nine samples, which presented distinct macroscopic appearances, as can be seen in Table 3.

Table 3. Reaction and gelation times for each prepared preceramic precursor together with corresponding macroscopic appearance after polymerization reaction by the sol-gel method

Preceramic precursor	Reaction time / min	Gelation time / days	Macroscopic appearance
MTES ₀	15	3	transparent
MTES _{0.1}	1440	4	white, opaque, vitreous
MTES _{0.5}	1800	4	white, opaque, vitreous
PTES ₀	15	3	white, crystalline
PTES _{0.1}	1800	7	white, opaque, chalk aspect
PTES _{0.5}	2160	15	white, opaque, chalk aspect
VTMS ₀	15	2	vitreous, yellow colorless
VTMS _{0.1}	120	3	opaque, brown colorless
VTMS _{0.5}	180	3	opaque, brown

Reaction and gelation times increased with the boron content irrespective of the precursor, with less pronounced influence for gelation time by considering the set of MTES and VTMS samples. However, Sorarù *et al.*²⁸ verified a contrary trend for gelation time related to the preparation of methyl-, vinyl- and ethyl-triethoxysilane-derived borosilicate gels. Boric acid participates of dissolution step, promoting the formation of the siloxane network, and behaves as a crosslinking agent. Similar results during the synthesis of poly(borosiloxane) gels from methyl-triethoxysilane and boric acid, with B/Si atomic ratios of 0.2 and 0.5, were also obtained by Siqueira *et al.*³³

Indeed, both increasing and decreasing trends of gelation times regarding boron content had already been reported.³⁷ According to Sorarù *et al.*,³⁸ when boron is inserted into alkoxy silane-derived polymeric structure

via $B(OSi)_3$ units, it behaves as a network former, with a reduction of the gelation times compared with the corresponding B-free polymeric gels. However, if the boron enters the polymeric network as non-bridging $B(OH)_3$ units, it behaves as an inert compound that dilutes the solution, decreasing the reaction rates and, consequently, resulting in longer gelation times.

By comparing the same boron content, reactions and gelling process were faster for VTMS- followed by MTES- and PTES-derived precursors. This behavior might be associated to steric hindrance promoted by the different organic groups during the hydrolysis and condensation reactions.²⁸

In the overall, B-free precursors were monolithic and transparent, meanwhile they became opaque as well as denser aspect with increasing of boron amount. A qualitative comparison among the three set of alkoxy silanes precursors revealed that those derived from PTES exhibited less stiffness. Probably, the steric hindrance promoted by the bulky phenyl groups resulted in lower crosslinking density giving rise to a softer polymer structure. VTMS-derived precursors exhibited higher stiffness when compared to the other samples. Macroscopically, this evidence suggests that vinyl groups allowed a more effective crosslinking of polymeric network.

Chemical structure

Polymerization reaction by the sol-gel method involving methyl-, phenyl- and vinyl-alkoxy silanes in the presence and absence of boric acid gave rise to the respective SiBOC and SiOC preceramic precursors, named poly(borosiloxanes) and poly(organosiloxanes), as represented in Figure 1.

Synthesis of poly(borosiloxanes) precursors from alkoxy silanes and boric acid (Figure 1a) is based on the

ability of $B(OH)_3$ species to hydrolyze the Si-OR groups producing reactive Si-OH moieties which can condense with B-OH bonds. As a result, boron atoms enter the siloxane network as trigonal BO_3 units via stable Si-O-B bonds.^{26,28,31} Furthermore, B-OH bonds can directly condense with Si-OR groups forming borosiloxane bonds and the corresponding alcohol molecule, ROH (methyl and ethyl alcohols in this case).⁴⁰

Preparation of poly(organosiloxane) precursors from alkoxy silanes initially involved the hydrolysis step catalyzed by acid medium, in which Si-OR groups are hydrolyzed to Si-OH silanol groups. Following, condensation occurred among the silanol groups formed generating a tridimensional inorganic network composed of Si-O-Si siloxane bonds, remaining the presence of organic group, R = methyl, phenyl or vinyl (Figure 1b).

Structural and thermal characterization

Fourier transform-infrared spectroscopy (FTIR)

FTIR spectra for each preceramic precursor system in the presence and absence of different B/Si atomic ratios are illustrated in Figure 2.

Broad absorption bands between 1200 and 1000 cm^{-1} (ν Si-O-Si) and around 460-400 cm^{-1} (δ Si-O),⁴⁷ typical of inorganic siloxane network, were verified for all precursors. Organic groups bonded to Si gave rise to bands highlighted in Figure 2 as # for Si-Me, * for Si-Ph and o for Si-Vi. The assignments and corresponding wavenumbers are reported in Table 4.²⁸ B-containing MTES-derived precursors revealed bands at 1300-1500, 1195 and 540 cm^{-1} , assigned to ν B-O, δ B-OH and δ O-B-O,⁴⁰ respectively. Furthermore, the most important band at 880 cm^{-1} is attributed to Si-O-B bridges in the polymer structure. B-containing PTES- and VTMS-derived precursors exhibited only some absorption bands corresponding to B-containing bonds (Figures 2b and 2c).

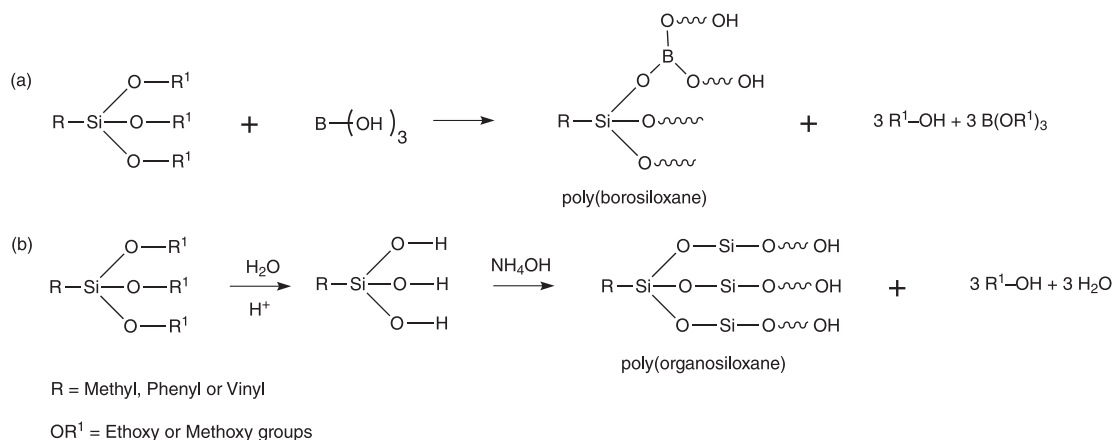


Figure 1. Proposed reactions by the sol-gel method illustrating the chemical structures for poly(borosiloxane) and poly(organosiloxane) preceramic precursors obtained with (a) and without (b) boric acid using methyl-, phenyl- and vinyl-alkoxy siloxanes.

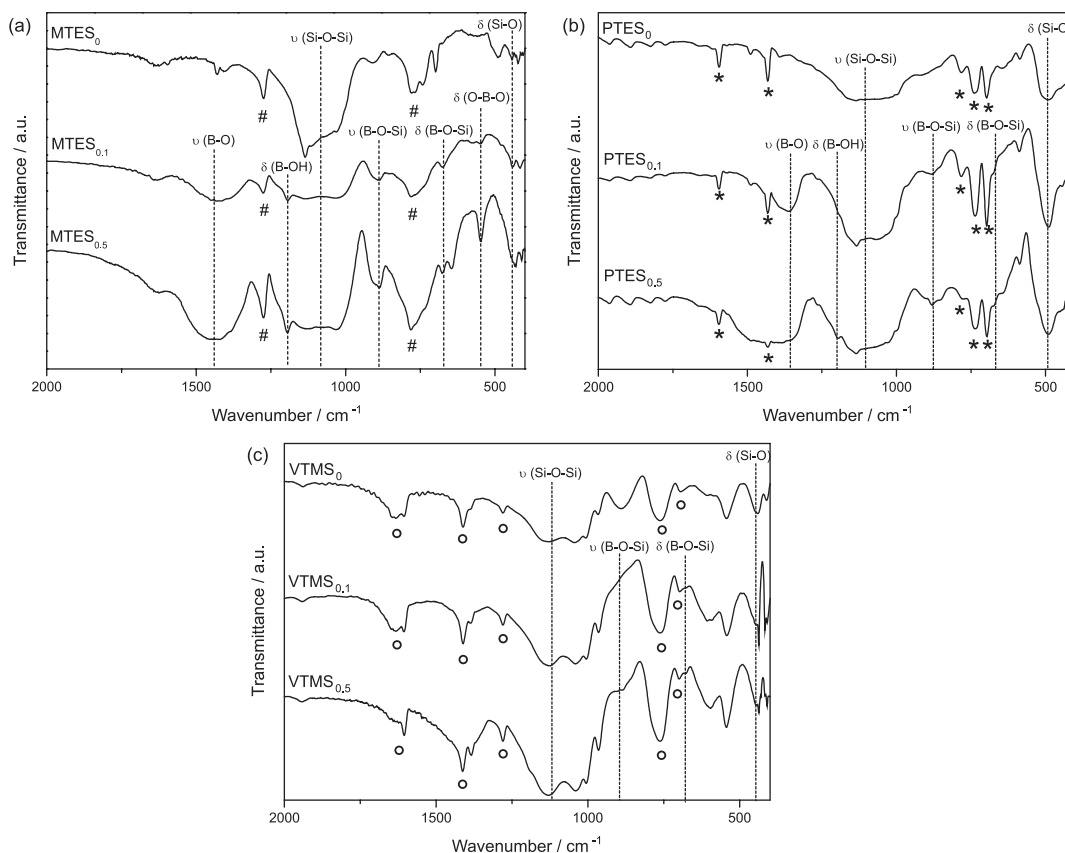


Figure 2. FTIR (KBr) spectra of preceramic precursors obtained by the sol-gel method from MTES (a), PTES (b) and VTMS (c), containing B/Si atomic ratios of 0, 0.1 and 0.5.

During the precursor's synthesis, particularly in gelling and drying steps, boron compounds evaporation usually takes place, decreasing the boron amount in the final polymeric gel, thus justifying the absence or smaller intensities bands.^{26,48} According to spectral profiles, by comparing the original absorption bands intensities, it seems that MTES precursors exhibited more intense bands corresponding to B-containing bonds when compared to other samples. This trend suggests that B–O–Si bonds were preferentially formed in the methyl groups-containing borosilicate gels.

A comparison involving different B/Si ratios in all alkoxysilanes-derived precursors revealed that the absorption band at around 880 cm^{-1} , assigned to borosiloxane bridges, increased with the B content. This result indicated that more trigonal boron units, composed of BO_3 , were incorporated into siloxane networks with increasing of boric acid amount²⁸ and this behavior was more evident for MTES-derived precursors and less pronounced for the VTMS system.

Thermogravimetry (TG)

Figure 3 displays TG curves for each preceramic precursor system in the presence and absence of different B/Si atomic ratios.

Table 4. FTIR absorption bands and respective assignments associated to the presence of organic groups bonded to Si in the MTES, PTES and VTMS preceramic precursors

Preceramic precursors system	Wavenumber / cm^{-1}	Assignment
MTES	1274	$\nu(\text{Si}-\text{CH}_3)$
	775	$\nu(\text{Si}-\text{C})$
PTES	1596	$\nu(\text{C}=\text{C})$
	1431	$\nu(\text{Si}-\text{Ph})$
	738	$\delta(\text{Si}-\text{Ph})$
	787	$\nu(\text{Si}-\text{C})$
	699	$\delta(\text{Si}-\text{Ph})$
VTMS	1630	$\nu(\text{C}=\text{C})$
	1412	$\nu(\text{Si}-\text{CH}=\text{CH}_2)$
	1280	$\nu(\text{Si}-\text{CH})$
	757	$\nu(\text{Si}-\text{C})$
	693	$\rho(\text{Si}-\text{CH}_2)$

MTES: methyltriethoxysilane; PTES: phenyltriethoxysilane; VTMS: vinyltrimethoxysilane.

In general, boron-free precursors revealed similar thermogravimetric profiles regarding to boron-containing samples and four main degradation steps were observed, with exception to PTES-derived precursors, which

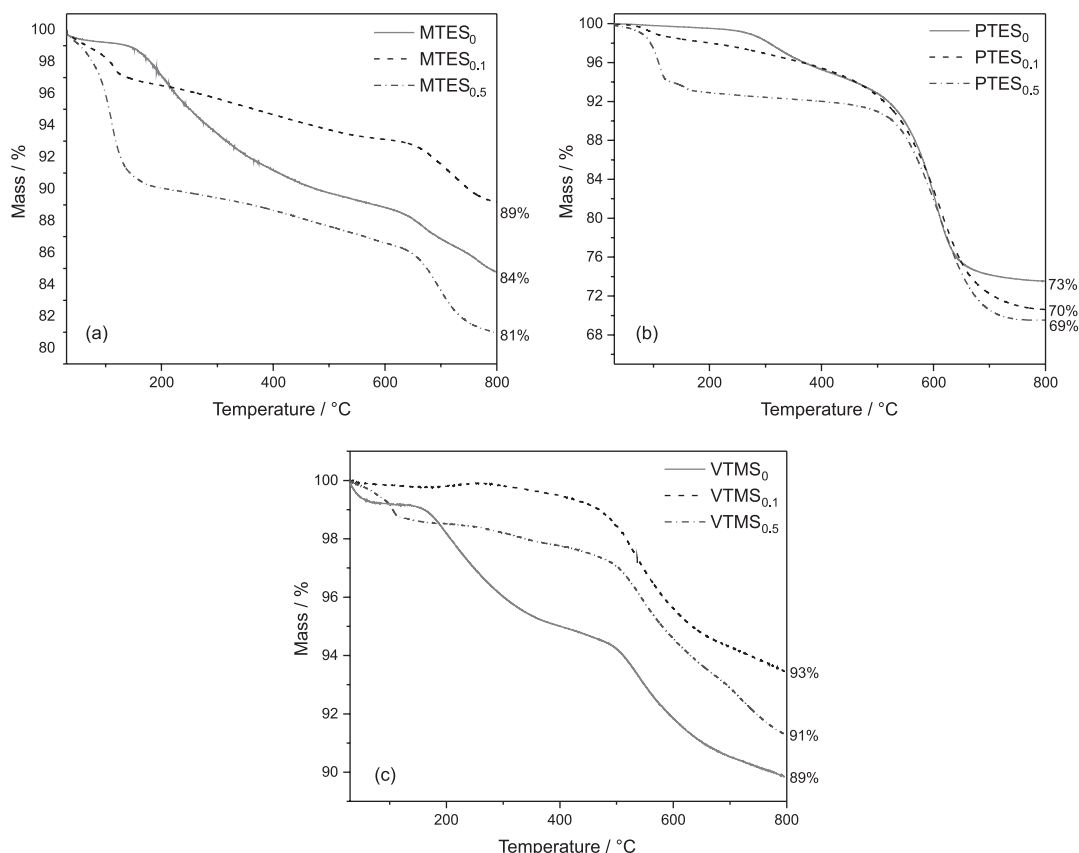


Figure 3. TG curves of preceramic precursors obtained by the sol-gel method from MTES (a), PTES (b) and VTMS (c), containing B/Si atomic ratios of 0, 0.1 and 0.5.

displayed three thermal decomposition events. The first event, occurred from room temperature to 150 °C, is related to evolution of water and alcohols, whilst the second evident event, from 150 to 300-400 °C, is attributed to evolution of free oligomers trapped in polymer structure, structural water, ethanol and methanol resulting of condensation reactions involving residual Si–OH, Si–OEt, Si–OMe and B–OH moieties and initial decomposition of organic groups.^{26,41} Furthermore, volatile boron compounds as well as boric acid molecules, that did not react during polymerization reaction, were also released in this temperature range.³⁵ The third less evident step, in the temperature range from 300-400 until 600 °C, is assigned to redistribution reactions between Si–O and Si–C bonds, releasing low molar mass oligomers and cyclic siloxanes.²⁶ The evident fourth step, occurred from 600 to 800 °C, is related to the polymer-to-ceramic conversion with the formation of corresponding silicon oxycarbide (SiOC) and boron silicon oxycarbide (SiBOC) glasses. This step is also associated with the cleavage of C–H and Si–C bonds, leading to the evolution of hydrogen and low molar mass hydrocarbons.^{26,30}

As expected, the initial mass loss was more pronounced for B-containing samples when compared to B-free

samples, due to boron compounds evolution, and this trend was proportional to boron amount. Considering the intermediary temperature range, the boron addition increased the thermal stability of polymer, indicating that boron atoms were incorporated into siloxane network. However, higher B contents revealed an opposite behavior for MTES_{0.5} and PTES_{0.5} samples. Probably, the less effective incorporation of boron for these respective systems are related to the absence of additional crosslinking and formation of a more opened polymeric network, as further described, which favored the greater evolution of boron compounds.

While PTES-derived precursors presented practically the same ceramic yield values, as shown at the last point of TG curves (Figure 3b), samples with B/Si = 0.1 exhibited higher values with respect to pure precursors for both MTES and VTMS systems (Figures 3a and 3c). The lowest ceramic yield values for B/Si = 0.5 are due to the more intense boron losses at low temperatures, as already stated.³³ By comparing the different sets of polymeric systems, the following decreasing order for ceramic yields was achieved, VTMS- > MTES- > PTES-derived precursors. The highest ceramic yield values for VTMS system were attributed to the polymerization of Si-vinyl groups during heat treatment,

resulting in additional crosslinking and, consequently, a more interconnected polymeric network.^{26,49}

Thermogravimetric profiles for PTES system, mainly regarding to third step occurred from 500 to 750 °C (Figure 3b), suggested a more opened network owing to empty spaces generated by the aromatic rings in the polymer structure. As consequence, more pronounced mass losses and less densely crosslinked precursors were obtained, in agreement with the macroscopic appearances (Table 3). However, the slower and continuous degradation of polymeric structure for both MTES and VTMS systems indicated that more packed polymeric networks were produced. Indeed, the highest ceramic yields for VTMS system (Figure 3c) together with the additional crosslinking promoted by the Si-vinyl groups justified the higher stiffness macroscopically observed.

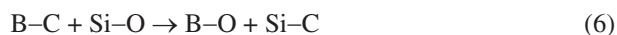
Characterization of SiOC and SiBOC ceramic materials

Fourier transform-infrared spectroscopy (FTIR)

Figure 4 exhibits FTIR spectra of SiOC and SiBOC ceramics derived from MTES, PTES and VTMS precursors (CMS, CPS and CVS ceramics), obtained at 1500 °C during 1 and 3 h annealing times. All ceramics presented spectral profiles typical of mineralized materials, evidenced by the absence of bands assigned to organic groups from alkoxysilanes precursors and presence of absorption bands corresponding to inorganic bonds. Broad bands at around 1086, 818 and 460 cm⁻¹, attributed to ν Si–O–Si, ν Si–C and δ Si–O,³² respectively, are typical of siloxane ceramic network, which were verified with different relative intensities according to each ceramic system. More intense bands at 818 cm⁻¹ (ν Si–C) with respect to those at 1086 cm⁻¹ (ν Si–O–Si) were mainly verified for the set of CPS ceramics, suggesting more effective phase segregation into ceramic matrix with the SiC formation, as expected after pyrolysis at 1500 °C.^{50,51} This trend, more evident for CPS ceramics, might be explained by the higher C_{free} amounts produced during heating treatment upon inert atmosphere for phenyl groups-containing precursors when compared to methyl and vinyl groups. Usually, inorganic precursors with aromatic and unsaturated organic groups attached at siloxane chain produce by degradation higher C_{free} contents in relation to saturated organic groups, giving rise to more effective production of SiC phase via carbothermal reduction reaction (equation 4).⁵² Effect of carbon content on structural properties of silicon carbon nitride (SiCN) was studied by atomistic simulations.⁵³ Indeed, the resulting structures showed a tendency to include a free carbon phase with increasing of the carbon content. Carbon rich regions became larger, resulting in

a network as the carbon content increases, as similarly verified in SiCO matrices. Further information on the local structure was provided by the Si–N–Si and C–C–C angular distributions, whose results indicated variations of Si–C bonds near the graphene layers when the sizes of carbon phases change. The proposed atomic model was employed to predict the structural as well as mechanical properties of SiCN materials at different compositions.

In general, B-containing ceramics revealed bands at ca. 1639, 1400, 887 and 680 cm⁻¹, related to the respective B–O–B bonds, ν B–O, ν B–O–Si and δ B–O–Si.³² These bands were more evident for CMS ceramics followed by the CPS and CVS systems, in agreement with the spectra profiles observed for the corresponding preceramic precursors (Figure 2), which suggested more effective boron incorporation for methyl-, phenyl- and vinyl-derived materials. Vibrational modes assigned to B–O and B–O–Si bonds, although less evident in some FTIR spectra, are probably associated to the redistribution reaction (equation 6) between B–C and Si–O bonds favored at high temperatures.³⁰



Apparently, more intense bands attributed to B-containing bonds were not verified with increasing boron content. Some bands related to borosiloxane bonds might be overlapped or a considerable portion of boron compounds was evaporated during the heating treatment at high temperatures,⁴⁸ preventing their visualization by FTIR technique.

X-ray diffraction (XRD)

Effect of boron content, organic substituent and annealing time on phase development of all ceramics was evaluated by X-ray diffraction, according to XRD patterns displayed in Figure 5.

CMS ceramics annealed for 1 h at 1500 °C (Figure 5a) revealed broad haloes at ca. 12° and 24° (2 θ), corresponding to a low ordering degree (+) and a random array of mixed silicon oxycarbide (SiO_xC_{4-x}, 1 ≤ x ≤ 3) and boron oxycarbide (BO_yC_{3-y}, 1 ≤ y ≤ 2) units (#) from respective SiOC and SiBOC ceramics.^{20,34} Broad diffraction signals at 35.5, 60 and 72° (2 θ), typical of SiC phase, were also detected.³¹ These signals became sharper as boron content increased, indicating more effective SiC crystallization, mainly at B/Si = 0.5. Furthermore, a broad hump around 43° (2 θ) assigned to the disordered carbon phase (*) was identified,¹⁵ with lower evidence for CMS_{0.1}-1h and CMS_{0.5}-1h when compared to CMS₀-1h. This probably suggests a higher consumption of residual carbon to

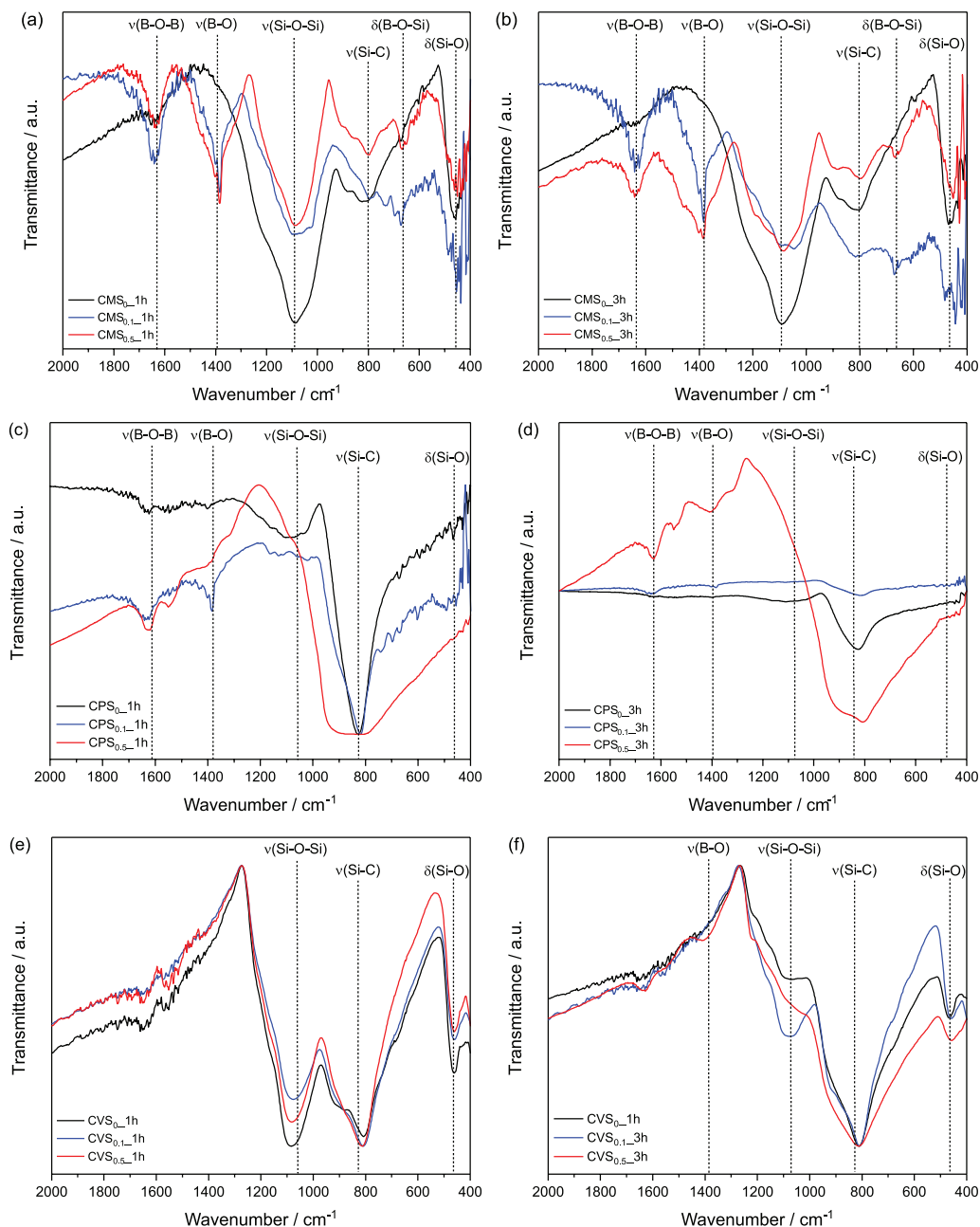


Figure 4. FTIR (KBr) spectra of CMS, CPS and CVS ceramics obtained by pyrolysis at 1500 °C during 1 h of the respective MTES-, PTES- and VTMS-derived precursors with B/Si atomic ratios of 0, 0.1 and 0.5 (a, c and e) and after 3 h annealing (b, d and f).

produce SiC phase in the B-containing ceramics. Similar XRD patterns for corresponding CMS ceramics annealed for 3 h were obtained (Figure 5b), practically indicating no crystallinity changes according to the annealing times evaluated.

Considerable crystallinity enhancement was achieved for the set of CPS ceramics (Figures 5c and 5d) in relation to CMS ceramics (Figures 5a and 5b). Much sharper and intense peaks assigned to SiC phase, together with the disappearance of amorphous portions (halo at $2\theta = 24^\circ$) and pronounced diminishing of low ordering degree region

(broad signal at $2\theta = 12^\circ$) were observed. Disordered carbon phase was also verified, which exhibited slightly sharper diffraction signals with boron content, indicating some graphitization degree.¹³ Graphitization of nanocrystalline graphite into SiBOC at 1500 °C, with the aid of boron, was reported by Peña-Alonso *et al.*⁴² Literature⁴² proposes that C atoms in the hexagonal graphene sheets are substituted by the B atoms resulting in BC₃ units, despite its mechanism is not completely understood. Therefore, boron addition associated to the carbon available for CPS ceramics contributed to crystallization of the SiC and residual carbon

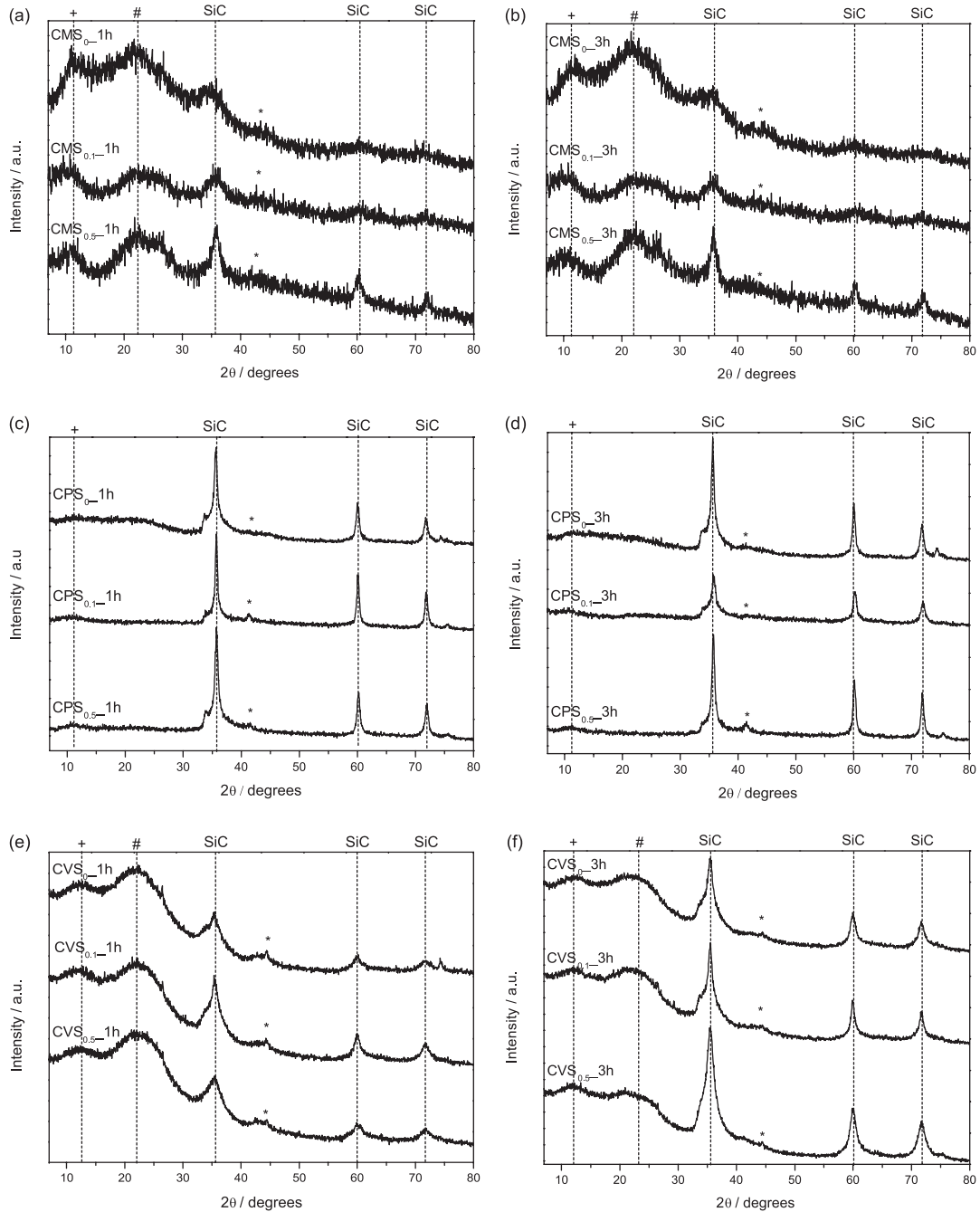


Figure 5. XRD patterns of CMS, CPS and CVS ceramics obtained by pyrolysis at 1500 °C during 1 h of the respective MTES-, PTES- and VTMS-derived precursors with B/Si atomic ratios of 0, 0.1 and 0.5 (a, c and e) and after 3 h annealing (b, d and f).

phases in different extent. A qualitative interpretation demonstrated no pronounced changes in XRD patterns, according to boron content and annealing time individually investigated, for CPS ceramics.

Intermediary crystallinity profiles for CVS ceramics (Figures 5e and 5f) were noticed by comparing the three ceramic systems. The same diffraction peaks and signals attributed to SiC and carbon phases as well as to amorphous and low ordering degree portions were detected, but with XRD patterns exactly comprised between CMS (Figures 5a

and 5b) and CPS (Figures 5c and 5d) ceramics. It seems that boron amount, but mainly the annealing time contributed to a more effective growth of SiC phase in relation to the same comparison for the other two set of ceramic samples.^{32,34,54}

A quantitative investigation over the different crystalline behaviors by considering the broadening line analysis, according to Scherrer equation, has been performed on the diffraction peak of SiC at 35.5° (2θ) and allows to estimate their average crystallite sizes, as compiled in Table 5 for all ceramics prepared.

Table 5. Average SiC crystallite sizes (t) values estimated from the broadening line analysis, according to Scherrer equation (equation 5)⁴⁵ on the diffraction peak at 35.5° (20) for CMS, CPS and CVS ceramics with and without boron pyrolyzed at 1500 °C for 1 and 3 h isothermal annealing

Ceramic material	t / nm
CMS ₀ _1h	0.87
CMS _{0.1} _1h	2.63
CMS _{0.5} _1h	7.44
CMS ₀ _3h	0.65
CMS _{0.1} _3h	2.40
CMS _{0.5} _3h	7.72
CPS ₀ _1h	13.40
CPS _{0.1} _1h	18.51
CPS _{0.5} _1h	13.81
CPS ₀ _3h	14.01
CPS _{0.1} _3h	11.42
CPS _{0.5} _3h	15.42
CVS ₀ _1h	2.49
CVS _{0.1} _1h	4.39
CVS _{0.5} _1h	4.94
CVS ₀ _3h	7.28
CVS _{0.1} _3h	9.73
CVS _{0.5} _3h	9.47

Indeed, CPS ceramics presented the largest SiC crystallites, followed by the CVS and CMS ceramic systems, as earlier stated from XRD patterns (Figure 5). This trend might be explained by the different residual carbon (C_{free}) amounts produced after pyrolysis, according to the organic substituent at alkoxysilane precursor structure. It is expected the following decreasing order related to C_{free} contents as a function of organic groups: phenyl > vinyl > methyl.^{37,55} Therefore, the higher carbon availability obtained in the phenyl groups-containing precursors possibly contributed to more effective production of SiC phase, resulting in larger nanocrystals, once carbon atoms in the neighboring of silicon atoms assist the formation of Si–C bonds⁵⁶ as well as by carbothermal reduction reaction (equation 4).^{20,21} Phase separation and free carbon structures were successfully reproduced by melt-quench simulation into amorphous SiBCO materials with different carbon contents.²⁵ An investigation of interface between free carbon and Si–O region of certain SiBCO composition revealed that the C atoms of graphitic layers only connect to Si atoms, and Si atoms form mixed bonds to C and O atoms with a tetrahedra geometry. The increasing of carbon content increases the amount of tetrahedrons with high C percentage, while decreases the proportion of Si–O₄ tetrahedron, justifying the *in situ* formation of rich Si–C bonds domains.

B-containing ceramics showed larger SiC nanocrystals compared to B-free ceramic samples. At high temperatures, typically around 1400 and 1500 °C, the presence of B in the silicon oxycarbide materials favors the consumption of the mixed Si (and mixed B in SiBOC) units, giving rise to a phase separation into SiC₄ and borosilicate clusters.⁴² The proportional increasing of SiC nanocrystals as boron content increases was more pronounced for CMS, followed by the CVS ceramics. These ceramics revealed major contributions of amorphous character (Figures 5a-5b and 5e-5f) and, mainly a destabilization effect in the silicon oxycarbide network due to their lower C_{free} contents.⁵⁶ Therefore, a more effective consumption of their mixed Si and B units probably took place, intensifying the boron action with the production of larger SiC nanocrystals. In contrast, non-proportional variations over crystallite sizes with the boron amount for CPS ceramics might be explained from their more crystalline profiles together with the higher free carbon amounts that stabilize the silicon oxycarbide structure at 1500 °C,⁵⁶ directly influencing the boron acting mechanism.

In the overall trend, larger SiC crystallites for ceramics annealed at 1500 °C during 3 h were obtained, with emphasis for CVS ceramics, despite some samples revealed an opposite result (Table 5). Sorarù *et al.*⁵⁷ investigated the effect of annealing at 1400 °C on the structural evolution of porous C-rich silicon(boron) oxycarbide glass. The authors obtained larger SiC crystallites (from 2.8 ± 0.2 to 3.5 ± 0.2 nm) and structural evolution of residual carbon phase, varying between turbostratic and graphitic structures, after holding times of 1 and 10 h, respectively. The nanostructural evolution was justified by the phase separation process, which occurs in the SiOC ceramic matrix at higher temperatures, as represented in equation 1. Consumption of mixed silicon oxycarbide units (SiO_xC_{4-x}, 1 ≤ x ≤ 3), present in higher amounts in the SiOC structure at low temperature, i.e., < 1200 °C, leads to a progressive increase of the SiC₄ and SiO₄ units, with subsequent progressive growth of the SiC nanocrystals, together with the ordering of the C_{free} phase. In this way, the opposite behaviors concerning SiC crystallite sizes verified for these B-containing and B-free ceramics might be related to the thermal degradation mechanisms and, subsequently, to phase separation processes occurred in structurally distinct precursors, producing silicon units in different extent.

X-ray photoelectron spectroscopy (XPS)

XPS measurements were carried out to get more insight into the chemical composition and bonding state on surface of the ceramic materials. All ceramics revealed peaks

typical for O-based bond (O1s peak), C-based bond (C1s peak), Si-based bond (Si2s and Si2p peaks) and B-based bond (B1s peak), this latter for B-containing samples,⁵⁸ which revealed different intensities according to ceramic system, boron content and annealing time, as illustrated in Figure 6.

O1s, C1s, Si2p and B1s peaks fittings are given in Figures 7 and 8 for CPS₀_1h and CPS_{0,1}_1h samples, respectively, to illustrate the corresponding components of ceramics in the absence and presence of boron. Basically, O1s peak fitting revealed O–C, O–Si, O–C=O and O–B bonds, whilst C1s exhibited Si–C and C–O bonds as well as

Csp³ and Csp². Deconvoluted Si2p and B1s peaks resulted in Si–C, Si–O, SiO₂, BC₂O, BCO₂, BOSi and B₂O₃ units.⁵⁹

Percentages corresponding to Csp², Csp³ and C_{free}, together with Si–O and Si–C bonds and different trigonal boron units were determined by the deconvoluted C1s, Si2p and B1s peaks integration for all ceramics, as shown in Table 6.

CPS ceramics revealed the highest and lowest percentages for Si–C and Si–O bonds, respectively, followed by CVS and CMS systems, confirming the enhanced crystallization for phenyl-groups containing samples by means of SiC phase production and simultaneous

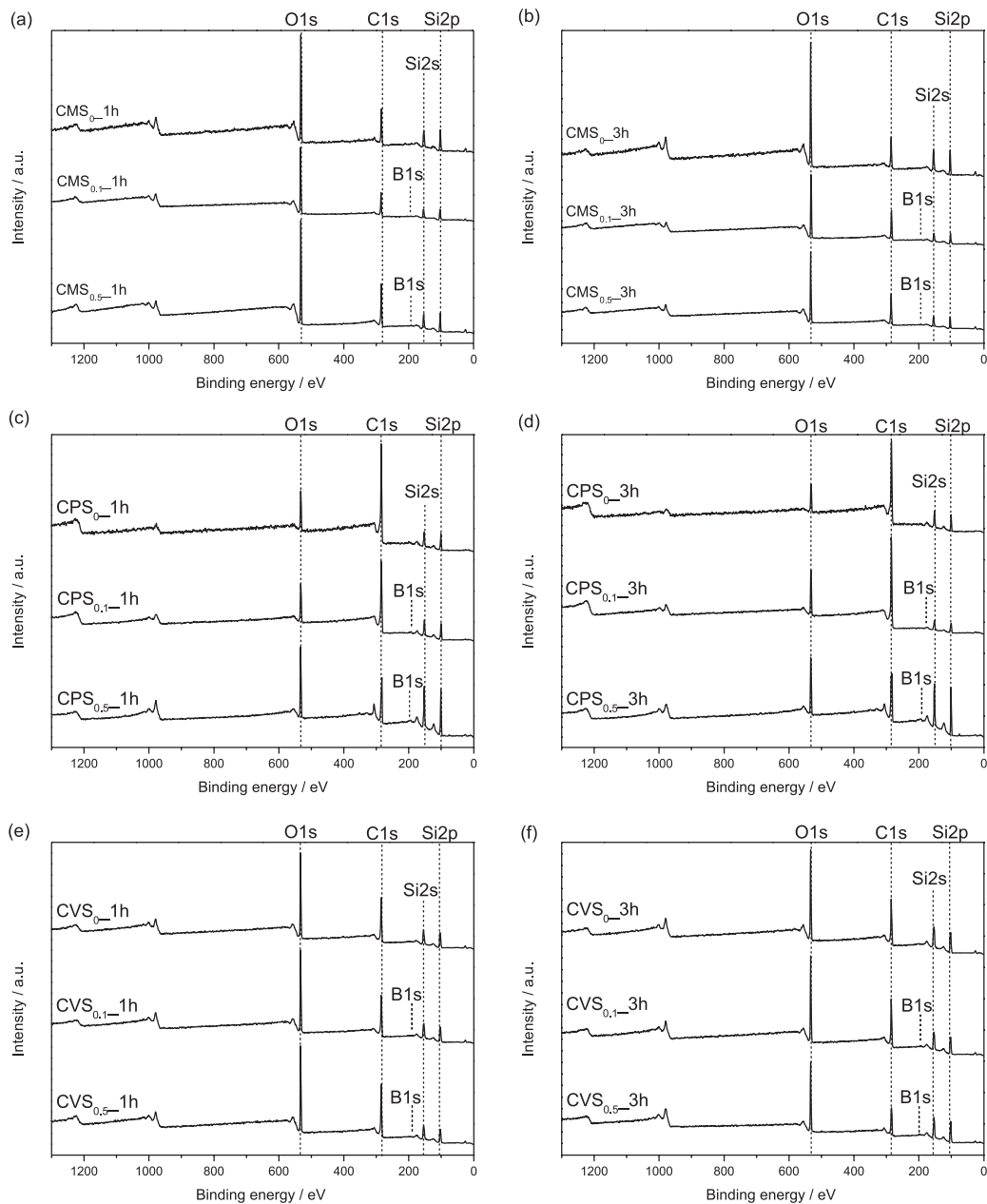


Figure 6. XPS survey spectra of CMS, CPS and CVS ceramics obtained by pyrolysis at 1500 °C during 1 h with B/Si atomic ratios of 0, 0.1 and 0.5 (a, c and e) and after 3 h annealing (b, d and f).

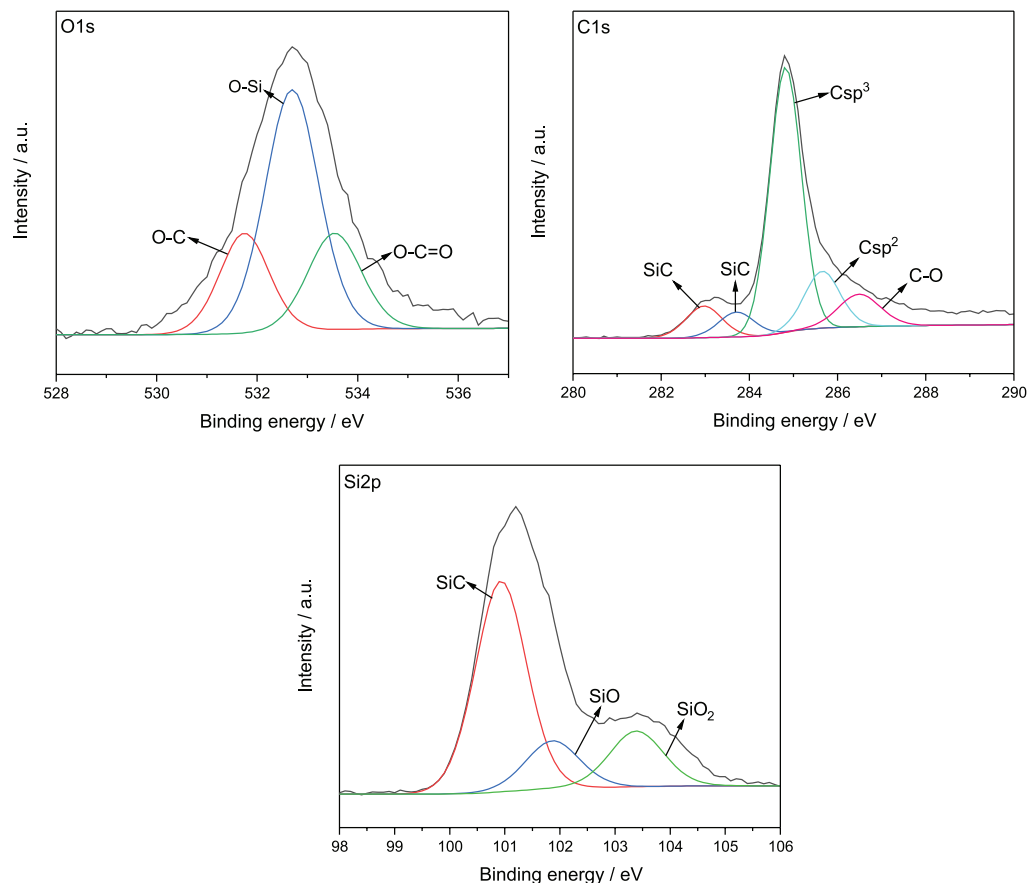


Figure 7. Deconvoluted XPS envelopes of CPS_{0-1h} sample for O1s, C1s and Si2p elements to illustrate different chemical species present into ceramics prepared.

diminishing of amorphous fraction composed of Si–O-rich bonds, as verified in XRD patterns (Figure 5 and Table 5). This trend also corroborated with FTIR spectra (Figures 4a-4d), in which more intense bands assigned to $\nu(\text{Si-C})$ and $\nu(\text{Si-O-Si})$ were verified for CPS and CMS, respectively.

By analyzing the total percentage of each element (Table 7), the highest and lowest carbon values were obtained for respective CPS and CMS, remaining intermediate values for CVS ceramics, corroborating with the different degradation profiles of organic groups present in the precursor structure, as observed by the TGA data. In the same way, oxygen percentages followed the trends earlier described for Si–O bond (CMS > CVS > CPS). Despite ceramics revealed no pronounced differences among C_{free} amounts (Table 6), C_{sp^2} was more effectively generated into CPS, whilst C_{sp^3} exhibited lower occurrence. Liao *et al.*²⁵ also found strong sp^2 carbon character together with a sp^3 character in the free carbon network of SiBCO materials with higher carbon content, by analyzing C–C–C angular distribution data. CMS ceramics showed exactly opposite results regarding CPS and intermediate C_{sp^2} and C_{sp^3} values for CVS were obtained. This indicates the

direct influence of organic substituent on conductive carbon phase development into resulting ceramics. Structural and electronic properties focusing on the behavior of lithiation of SiCO with different carbon contents employing first-principles calculations were reported by Liao *et al.*⁶⁰ The results revealed amorphization of lithiated structures during the process of Li insertion and preference of Li atoms to bond with oxygen atoms. C–C bonds were favored in the SiCO structures with high carbon contents and most of the Li atoms were accommodated near the free carbon structure in SiCO, indicating a larger lithium capacity as an anode of a Li-ion battery for C-enriched SiCO. Furthermore, band gap value diminished with increasing C content, reflecting the great influence of free carbon network on electrochemical response.

B-containing ceramics were composed of BC_2O , BCO_2 and BOSi bonds, with higher proportions for the latter unit, confirming the effective formation of borosiloxane bonds into SiBOC materials after boron addition. CPS ceramics revealed preferential formation of B–O–Si bonds, due to their higher percentage values, followed by CMS and CVS, although the FTIR spectra have indicated a slightly different preference order for borosiloxane bonds,

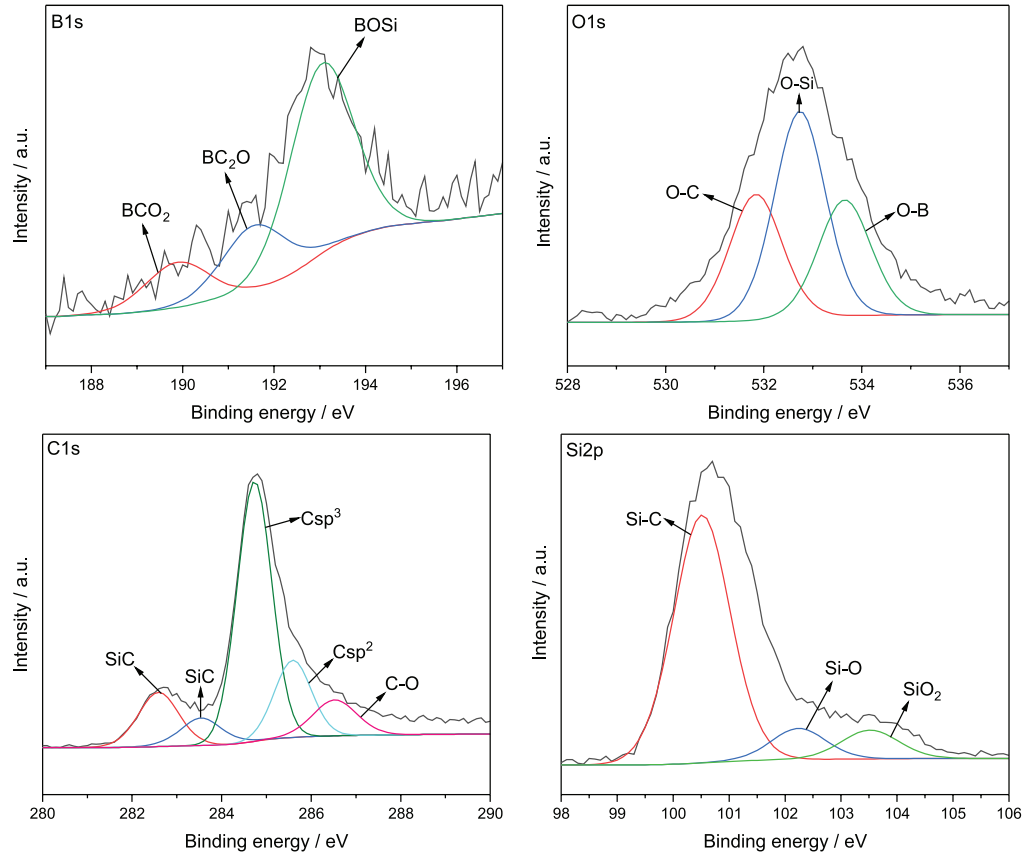


Figure 8. Deconvoluted XPS envelopes of CPS_{0.1-1h} sample for B1s, O1s, C1s and Si2p elements to illustrate different chemical species present into ceramics prepared.

Table 6. Percentages for Csp², Csp³ and C_{free}, together with Si-C and Si-O bonds and different trigonal boron units, obtained from deconvoluted C1s, Si2p and B1s peaks integration, for CMS, CPS and CVS ceramics with and without boron pyrolyzed at 1500 °C during 1 and 3 h annealing

Ceramic material	Percentage / %								
	Csp ³	Csp ²	C _{free} ^a	SiC	SiO	BC ₂ O	BCO ₂	BOSi	B ₂ O ₃
CMS _{0_1h}	42.70	28.61	71.31	16.74	21.40	–	–	–	–
CMS _{0.1-1h}	37.00	29.35	66.35	14.29	20.35	20.64	24.60	54.76	–
CMS _{0.5-1h}	36.81	27.54	64.35	5.36	10.00	9.43	26.97	63.03	–
CMS _{0_3h}	32.05	27.23	59.28	14.73	21.03	–	–	–	–
CMS _{0.1-3h}	39.91	25.65	65.56	14.66	13.26	16.31	35.31	47.88	–
CMS _{0.5-3h}	31.68	26.17	57.85	7.85	11.77	9.52	32.16	58.32	–
CPS _{0_1h}	12.66	51.33	63.99	65.74	15.83	–	–	–	–
CPS _{0.1-1h}	14.63	46.13	60.76	80.71	9.83	15.05	21.53	63.42	–
CPS _{0.5-1h}	11.32	17.24	28.56	82.72	11.94	21.15	17.27	26.43	35.15
CPS _{0_3h}	11.38	50.50	61.88	88.32	9.26	–	–	–	–
CPS _{0.1-3h}	14.09	53.61	67.70	58.84	10.73	12.80	22.18	64.43	–
CPS _{0.5-3h}	16.27	27.11	43.38	92.41	7.59	16.55	19.72	63.73	–
CVS _{0_1h}	20.48	46.98	67.46	31.33	10.76	–	–	–	–
CVS _{0.1-1h}	25.51	31.94	57.45	31.35	15.93	100.00	–	–	–
CVS _{0.5-1h}	22.64	35.87	58.51	33.73	12.54	18.95	30.68	50.36	–
CVS _{0_3h}	19.10	37.59	56.69	36.96	19.89	–	–	–	–
CVS _{0.1-3h}	15.29	39.80	55.09	41.59	18.16	100.00	–	–	–
CVS _{0.5-3h}	14.85	24.67	39.52	50.51	21.78	24.16	27.38	48.46	–

^aC_{free} = Csp² + Csp³

Table 7. Total percentage of carbon, oxygen, silicon and boron, obtained from deconvoluted C1s, O1s, Si2p and B1s peaks integration, for CMS, CPS and CVS ceramics with and without boron pyrolyzed at 1500 °C during 1 and 3 h annealing

Ceramic material	Total percentage / %			
	C	O	Si	B
CMS ₀ _1h	37.31	37.00	25.69	–
CMS _{0.1} _1h	37.93	38.71	21.38	0.95
CMS _{0.5} _1h	43.09	36.55	19.24	1.12
CMS ₀ _3h	29.96	42.16	27.88	–
CMS _{0.1} _3h	44.90	34.08	19.55	1.48
CMS _{0.5} _3h	45.36	34.99	18.76	0.85
CPS ₀ _1h	74.58	12.43	12.99	–
CPS _{0.1} _1h	68.80	14.06	15.36	1.78
CPS _{0.5} _1h	40.36	21.27	35.05	1.74
CPS ₀ _3h	76.53	10.06	13.41	–
CPS _{0.1} _3h	73.61	14.47	10.66	1.25
CPS _{0.5} _3h	49.61	16.80	31.41	1.49
CVS ₀ _1h	44.97	31.58	23.45	–
CVS _{0.1} _1h	43.21	30.45	24.21	1.79
CVS _{0.5} _1h	49.12	28.56	20.54	1.78
CVS ₀ _3h	45.64	27.89	25.26	–
CVS _{0.1} _3h	41.58	28.92	28.92	0.72
CVS _{0.5} _3h	37.88	28.98	31.41	1.20

CMS > CPS > CVS (Figure 4). Interestingly, among the B-containing species, B₂O₃ phase was verified only for CPS_{0.5}_1h. Higher carbon amounts into matrix, as verified for CPS, favor SiC bonds due to greater affinity between silicon and carbon, making boron more susceptible to linkage with oxygen atoms.²⁶ The absence of this phase in other samples might be related to the total boron amount after pyrolysis, which varied from 0.72 to 1.79% (Table 7).

Neither all ceramic samples revealed higher boron contents with increasing B/Si ratio, indicating loss of this element during the incorporation process in the gelation step. In these cases, most of boron atoms available were still in the acid form, which suffered condensation in the drying step.^{26,48} However, as the B/Si ratio increased, B–O–Si proportions increased for CMS and diminished for CVS (Table 6), which were compatible with FTIR spectra for these sets of ceramics (Figures 4a–4b and 4e–4f). The results pointed out to the effective formation of covalent bonds in Si–O–C and Si–B–O–C matrices in different extent, according to ceramic system, showing homogeneous boron incorporation via B–O–Si borosiloxane bonds.

Ceramic samples annealed for 3 h revealed higher SiC percentages regarding the analogous obtained during 1 h, evidencing the crystallization process of silicon carbide

phase as slightly stated in the XRD patterns. By comparing the two annealing conditions, higher proportions ascribed to BCO₂ when compared to BC₂O units were clearly verified, whilst BOSi increased for CPS and remained practically constant for CMS and CVS ceramics. These results were compatible with redistribution reactions between Si–O and B–C bonds, giving rise to B–O- and Si–C-rich phases (equation 6). The evident increase in borosiloxane bonds for CPS possibly was related to more effective SiC crystallization earlier confirmed, with simultaneous formation of B–O units.

Therefore, SiC and C_{graphitic} phases produced in different proportions into ceramic materials based on the Si–O–C and Si–B–O–C systems, according to organic substituent at alkoxy silanes structure in the presence and absence of boron, demonstrated potentialities for applications as electrochemical sensors and Li-ion batteries.

Conclusions

SiOC and SiBOC ceramics were successfully prepared from pyrolysis route of MTES, PTES and VTMS precursors, with and without boric acid, at 1500 °C during 1 and 3 h isothermal annealing. Crystallization and composition on ceramics were evaluated in terms of organic substituent nature, boron content and annealing time.

Different crystalline profiles were noticed according to ceramic system investigated. Enhanced SiC phase crystallization for PTES-derived ceramics, followed by those containing VTMS and MTES, also confirmed by XPS measurements from percentages of bands assigned to Si–C and Si–O bonds, was attributed to carbon content in each polymer precursor. Csp² and Csp³ widely varied according to precursor chemistry, revealing the highest and the lowest amounts for phenyl-groups containing ceramics, whilst those composed of methyl groups showed opposite results.

Boron was incorporated into SiBOC materials via stable borosiloxane bonds, in different extent, which were confirmed through percentages of BOSi bonds according to ceramic system. Preference order for borosiloxane bonds was given from ceramics containing the following groups: methyl > phenyl > vinyl. Lower boron amounts incorporated into some ceramics were related to boron compounds evaporation during the gelation step. Furthermore, boron addition induced the growth of SiC crystallites, having more influence for ceramics exhibiting higher proportion of amorphous fraction and lower residual carbon amount. In the overall, the annealing time induced the growth of SiC phase and diminished the C_{free} content, probably due to higher consumption of carbon domains to produce Si–C bonds containing phase.

In summary, the combined use of boron and alkoxy silanes containing different organic substituents played a promising synthetic strategy to fabricate multicomponent ceramics with varied proportions of semiconducting SiC and conductive C_{graphitic} phases. Therefore, the produced ceramics by this approach revealed potentialities for applications in which electrical characteristics are required.

Acknowledgments

The authors acknowledge the financial support from CAPES (Brazil), CNPq (Brazil), grant 309116/2016-3, together with the ESPEC (Brazil), LARX (Brazil) and LADEMA (Brazil) laboratories from UEL and Photoelectron Spectroscopy Laboratory in the X-Ray Region-XPS from IQ/UFRJ.

Author Contributions

Mariana G. Segatelli was responsible for conceptualization, formal analysis, funding acquisition, project administration, resources, supervision, writing original draft, writing review and editing; Patrícia M. Sanchez for methodology, data curation, formal analysis; Lívia R. C. Silva for data curation, formal analysis, writing original draft; Maria A. Silva for formal analysis, writing review and editing; César R. T. Tarley for formal analysis, funding acquisition, resources, writing review and editing; Paulo R. C. da Silva for data curation, formal analysis, writing-review and editing; Emerson S. Ribeiro for data curation, formal analysis, writing-review and editing.

References

- Colombo, P.; Mera, G.; Riedel, R.; Sorarù, G. D.; *J. Am. Ceram. Soc.* **2010**, *93*, 1805.
- Wen, Q.; Yu, Z.; Riedel, R.; *Prog. Mater. Sci.* **2020**, *109*, 100623.
- Wang, X.; Gong, C.; Fan, G.; *Mater. Res. Bull.* **2011**, *46*, 2398.
- Chlup, Z.; Černý, M.; Strachota, A.; Sucharda, Z.; Halasová, M.; Dlouhý, I.; *J. Eur. Ceram. Soc.* **2014**, *34*, 3389.
- Mazo, M. A.; Padilla, I.; Tamayo, A.; Robla, J. I.; López-Delgado, A.; Rubio, J.; *Sol. Energy* **2018**, *173*, 256.
- Yang, H.; Li, C.; Yue, X.; Huo, J.; Ye, F.; Liu, J.; Shi, F.; Ma, J.; *Mater. Des.* **2020**, *185*, 108217.
- Tahir, M. S.; Weinberger, M.; Balasubramanian, P.; Diemant, T.; Behm, R. J.; Lindén, M.; Wohlfahrt-Mehrens, M.; *J. Mater. Chem. A* **2017**, *5*, 10190.
- Godoy, N. V.; Pereira, J. L.; Duarte, E. H.; Tarley, C. R. T.; Segatelli, M. G.; *Mater. Chem. Phys.* **2016**, *175*, 33.
- Memon, F. A.; Morichetti, F.; Cantoni, M.; Somaschini, C.; Asa, M.; Bertacco, R.; Chowdhry, B. S.; Melloni, A.; *J. Lightwave Technol.* **2020**, *38*, 784.
- Flores, L. F.; Tucto, K. Y.; Guerra, J. A.; Töfflinger, J. A.; Serquen, E. S.; Osvet, A.; Batentschuk, M.; Winnacker, A.; Grieseler, R.; Weingärtner, R.; *Opt. Mater.* **2019**, *92*, 16.
- Li, X.; Feng, J.; Jiang, Y.; Li, L.; Feng, J.; *Ceram. Int.* **2019**, *45*, 9704.
- Bik, M.; Gil, A.; Stygar, M.; Dąbrowa, J.; Jeleń, P.; Długóń, E.; Leśniak, M.; Sitarz, M.; *Intermetallics* **2019**, *105*, 29.
- Zhang, Z.; Bao, Y.; Sun, X.; Chen, K.; Zhou, M.; He, L.; Huang, Q.; Huang, Z.; Chai, Z.; Song, Y.; *ACS Omega* **2020**, *5*, 11100.
- Schelm, K.; Morales, E. A.; Scheffler, M.; *Materials* **2019**, *12*, 1870.
- Iastrenski, M. F.; da Silva, P. R. C.; Tarley, C. R. T.; Segatelli, M. G.; *Ceram. Int.* **2019**, *45*, 21698.
- Sasikumar, P. V. W.; Zera, E.; Graczyk-Zajac, M.; Riedel, R.; Soraru, G. D.; Dunn, B.; *J. Am. Ceram. Soc.* **2016**, *99*, 2977.
- Duan, L.; Ma, Q.; *Ceram. Int.* **2012**, *38*, 2667.
- Oteo, J. L.; Mazo, M. A.; Palencia, C.; Rubio, F.; Rubio, J.; *J. Nano Res.* **2011**, *14*, 27.
- Yang, X.; Jiang, P.; Sun, F.; Yang, L.; Fan, X.; *Ceram. Int.* **2020**, *46*, 10392.
- Schiavon, M. A.; Ferrari, J. L.; Hojamberdiev, M.; Yoshida, I. V. P.; *Quim. Nova* **2015**, *38*, 972.
- Stabler, C.; Ionescu, E.; Graczyk-Zajac, M.; Gonzalo-Juan, I.; Riedel, R.; *J. Am. Ceram. Soc.* **2018**, *101*, 4817.
- Saha, A.; Raj, R.; *J. Am. Ceram. Soc.* **2007**, *90*, 578.
- Sorarù, G. D.; Pena-Alonso, R.; Leoni, M.; *Microporous Mesoporous Mater.* **2013**, *172*, 125.
- Kleebe, H.-J.; Blum, Y. D.; *J. Eur. Ceram. Soc.* **2008**, *28*, 1037.
- Liao, N.; Xue, W.; Zhou, H.; Zhang, M.; *J. Alloys Compd.* **2014**, *610*, 45.
- Sreejith, K. J.; Prabhakaran, P. V.; Laly, K. P.; Dimple, R.; Packirisamy, S.; *Ceram. Int.* **2016**, *42*, 15285.
- Klonczynski, A.; Schneider, G.; Riedel, R.; Theissmann, R.; *Adv. Eng. Mater.* **2004**, *6*, 64.
- Sorarù, G. D.; Babonneau, F.; Gervais, C.; Dallabona, N.; *J. Sol-Gel Sci. Technol.* **2000**, *18*, 11.
- Liebau, V.; Hauser, R.; Riedel, R.; *C. R. Chim.* **2004**, *7*, 463.
- Zhang, X.; Liu, C.; Hong, C.; Han, J.; Han, W.; Du, S.; *Ceram. Int.* **2015**, *41*, 15292.
- Gencer, A.; Oksal, B. S.; *J. Sol-Gel Sci. Technol.* **2014**, *73*, 171.
- Tamayo, A.; Peña-Alonso, R.; Rubio, F.; Rubio, J.; Oteo, J. L.; *J. Non-Cryst. Solids* **2012**, *358*, 155.
- Siqueira, R. L.; Yoshida, I. V. P.; Pardini, L. C.; Schiavon, M. A.; *Mater. Res.* **2007**, *10*, 147.
- Schiavon, M. A.; Gervais, C.; Babonneau, F.; Soraru, G. D.; *J. Am. Ceram. Soc.* **2004**, *87*, 203.

35. Bai, H. W.; Wen, G.; Huang, X. X.; Han, Z. X.; Zhong, B.; Hu, Z. X.; Zhang, X. D.; *J. Eur. Ceram. Soc.* **2011**, *31*, 931.
36. Wang, L.; Lu, K.; Ma, R.; *Appl. Phys. A: Mater. Sci. Process.* **2019**, *125*, DOI: 10.1007/s00339-019-2680-z.
37. Cordelair, J.; Greil, P.; *J. Eur. Ceram. Soc.* **2000**, *20*, 1947.
38. Sorarù, G. D.; Dallabona, N.; Gervais, C.; Babonneau, F.; *Chem. Mater.* **1999**, *11*, 910.
39. Gervais, C.; Babonneau, F.; Dallabona, N.; Sorarù, G. D.; *J. Am. Ceram. Soc.* **2001**, *84*, 2160.
40. Peña-Alonso, R.; Sorarù, G. D.; *J. Sol-Gel Sci. Technol.* **2007**, *43*, 313.
41. Trezza, M. A.; *Mater. Res.* **2007**, *10*, 331.
42. Peña-Alonso, R.; Mariotto, G.; Gervais, C.; Babonneau, F.; Soraru, G. D.; *Chem. Mater.* **2007**, *19*, 5694.
43. Wen, Q.; Xu, Y.; Xu, B.; Fasel, C.; Guillon, O.; Buntkowsky, G.; Yu, Z.; Riedel, R.; Ionescu, E.; *Nanoscale* **2014**, *6*, 13678.
44. Xu, T.; Ma, Q.; Chen, Z.; *Ceram. Int.* **2011**, *37*, 2555.
45. Ionescu, E.; Kleebe, H. J.; Riedel, R.; *Chem. Soc. Rev.* **2012**, *41*, 5032.
46. Cullity, B. D.; Stock, S. R.; *Elements of X-Ray Diffraction*, 3rd ed.; Pearson Education Limited: London, UK, 2014.
47. Larson, G. L.; Arkles, B.; *Silicon Compounds: Silanes and Silicones*, 3rd ed.; Gelest Inc.: Morrisville, 2013, p. 175.
48. Shawgi, N.; Li, S. X.; Wang, S.; Wang, Z.; Nie, Y. N.; *J. Sol-Gel Sci. Technol.* **2017**, *82*, 450.
49. Ambadas, G.; Packirisamy, S.; Ninan, K. N.; *J. Mater. Sci. Lett.* **2002**, *21*, 1003.
50. Hasik, M.; Wójcik-Bania, M.; Nyczyk, A.; Gumuła, T.; *React. Funct. Polym.* **2013**, *73*, 779.
51. Mazo, M. A.; Tamayo, A.; Rubio, F.; Soriano, D.; Rubio, J.; *J. Non-Cryst. Solids* **2014**, *391*, 23.
52. Mazo, M. A.; Tamayo, A.; Rubio, J.; *J. Eur. Ceram. Soc.* **2016**, *36*, 2443.
53. Liao, N.; Xue, W.; Zhang, M.; *J. Eur. Ceram. Soc.* **2012**, *32*, 1275.
54. Wang, Y.; Li, H.; Zhang, L.; Cheng, L.; *Ceram. Int.* **2009**, *35*, 1129.
55. Fukui, H.; Ohsuka, H.; Hino, T.; Kanamura, K.; *ACS Appl. Mater. Interfaces* **2010**, *2*, 999.
56. Brequel, H.; Parmentier, J.; Sorarù, G. D.; Schiffini, L.; Enzo, S.; *Nanostruct. Mater.* **1999**, *11*, 721.
57. Sorarù, G. D.; Pena-Alonso, R.; Kleebe, H. J.; *J. Eur. Ceram. Soc.* **2012**, *32*, 1751.
58. Lewandowska-Łańcucka, J.; Staszewska, M.; Szuwarzyński, M.; Zapotoczny, S.; Kepczynski, M.; Olejniczak, Z.; Sulikowski, B.; Nowakowska, M.; *Mater. Des.* **2018**, *146*, 57.
59. Lyu, Y.; Tang, H.; Zhao, G.; *J. Eur. Ceram. Soc.* **2020**, *40*, 324.
60. Liao, N.; Zheng, B.; Zhou, H.; Xue, W.; *J. Mater. Chem. A* **2015**, *3*, 5067.

Submitted: October 13, 2020

Published online: February 17, 2021

